Modelling the Electrical Activity of the Heart

Sergio Alonso and Rodrigo Weber dos Santos

Abstract The electrocardiogram signal is a popular measurement of the electrical activity of the whole heart. It reflects the interaction and diversity of the electrical activity of cells from different parts of the heart. Rhythmically each cell changes the value of the transmembrane potential, and this change in the electrical properties of the cell propagates through the tissue producing the coordination of the electrical signal, which triggers the contraction of the whole heart. In this chapter we show the main ingredients for the description of the electrophysiology of a single cell and the different models for the propagation of the electrical signal along cardiac tissue. We discuss the main characteristics of certain arrhythmias and the corresponding patterns of electrical activity obtained in the numerical simulations.

1 Introduction

As excitable cells, cardiac myocytes are able to respond to an external stimulus with the generation of an Action Potential (AP), i.e. a specific signature of the transmembrane potential that varies along time for a certain characteristic duration, called Action Potential Duration (APD). The excitation appears only for stimulus over a certain threshold, resulting in an AP with always the same shape and leaving a refractory state which precludes a fast re-excitation of the cell [1, 2].

S. Alonso (✉)
Department of Physics, Universitat Politècnica de Catalunya, Barcelona, Spain
e-mail: s.alonso@upc.edu

R. W. dos Santos
Department of Computer Science, Universidade Federal de Juiz de Fora, Juiz de Fora, Brazil
e-mail: rodrigo.weber@ufjf.edu.br

S. Golemati and K. S. Nikita (eds.), *Cardiovascular Computing—Methodologies and Clinical Applications*, Series in BioEngineering,
https://doi.org/10.1007/978-981-10-5092-3_10

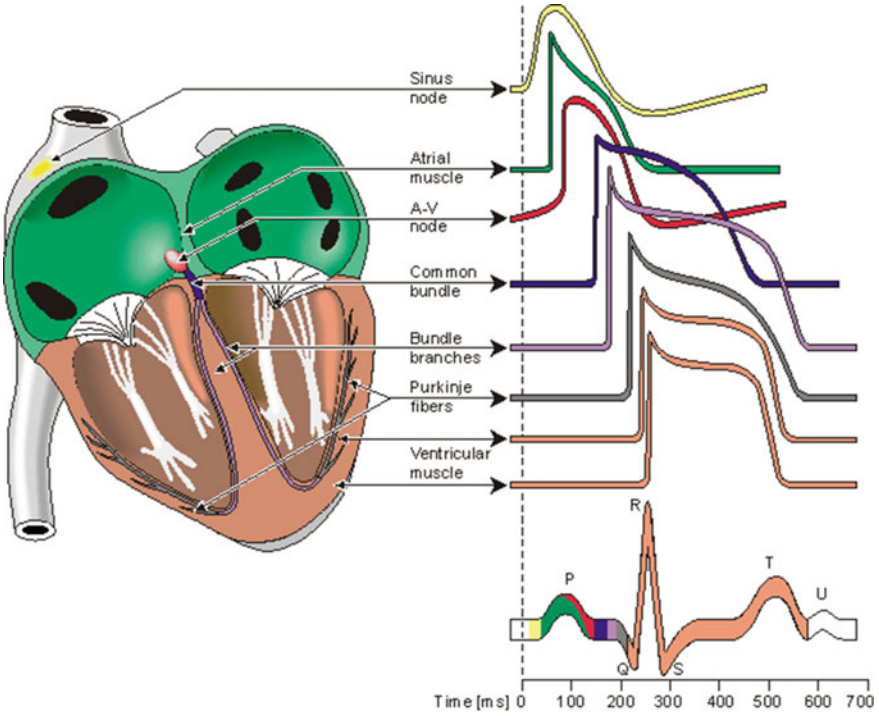

Fig. 1 Location of the different parts of the heart and relation of the electrocardiogram with the action potential curves in different types of myocytes. Reprinted from the free open access book [3]

In the heart, the AP has the important role of the synchronization of the whole cardiac tissue. To work as an efficient pump, the myocytes have to contract in a synchronized fashion. To this end, once an AP is initiated in a particular region (the sinoatrial node, SAN) it propagates from one cell to its neighbours, until all the cells of the heart are excited. The atria first pumps the blood to the ventricles, which later pumps blood out of the heart. The region that electrically connects the atria to the ventricles, called atrioventricular node (AVN), slows down the AP propagation so that the trigger for contraction arrives later in the ventricle than in the atria, see Fig. 1 [3]. A loss of synchronization of cardiac electrical impulses controlling the pumping of blood is associated with a number of arrhythmias including atrial (AF), ventricular (VF) fibrillation, and ventricular tachycardia (VT).

The electrical activity of the heart is visible in the electrocardiogram (ECG). A series of electrodes record the small voltage changes on the thorax of a person. With the ECG both the rhythm and the morphology of the electrical activity is recorded. The different phases of propagation along the heart leave different traces in the ECG, see Fig. 1. Thus, anomalies in propagation result in distinctive shape variations in the ECG.

Together with the ECG, there are other valuable experimental methods like optical imaging of the voltage and calcium content and electrophysiological studies, both at different scales ranging from individual cells to cardiac tissue, which permit the development of detailed cardiac models [4].

The modelling of the electrical properties of the cardiac tissue is the main purpose of this chapter. Computational models of the cardiac tissue are useful tools for the characterization of different mechanisms of arrhythmias; the definition of new effective defibrillation protocols; the effects of the different pathologies on cardiac tissue, like ischemia and fibrosis; the study of the effects of anti-arrhythmic drugs; and even the effects of genetic mutations on the behaviour of ion channels.

This chapter is organized as follows: in the next section, we present the basic ingredients to model the genesis of AP in cardiac myocytes. We show some simulation examples of myocytes located in different parts of the heart in Sect. 3. In Sect. 4, we discuss models for the propagation of AP in cardiac tissue. Such models of tissue are employed to describe wave propagation and different types of arrhythmias in Sect. 5. Finally, Sect. 6 provides a short discussion and outlook for future perspectives.

2 Celular Modelling

Cardiac myocytes are electrically active cells, or excitable cells, of the heart. They have a length of 100–120 μm and a diameter of 10–20 μm. Each myocyte is separated from the extracellular space by a phospholipid bilayer membrane. This cellular membrane permits the flow of some ions (Na^+, K^+, Ca^{2+}, Cl^-) between the extracellular and intracellular media through specific ion channels. The resulting different ionic concentrations between the interior and the exterior of the cell generates a transmembrane potential difference, i.e. a potential difference across the cell membrane. AP produces myocyte contraction because it triggers a pulse of intracellular Calcium concentration, $[Ca]_i$. The increase of $[Ca]_i$, enables the cellular contraction machinery to work, via crossbridge cycling tropomyosin slides over actin filaments and shortens the myocyte length. Figure 2 presents the typical waveforms of AP,

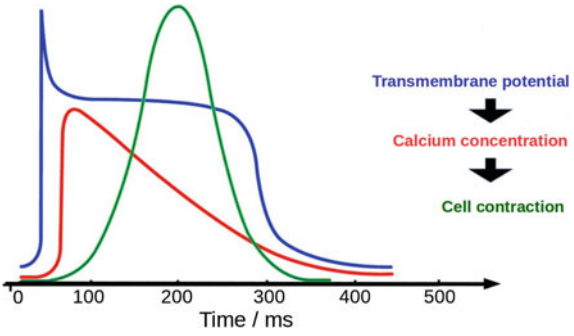

Fig. 2 Sequence of the processes inside a cardiac myocyte. First the transmembrane potential depolarizes, followed by an increase in Ca^{2+} concentration in the cytosol and the final contraction of the cell

$[Ca]_i$ pulse and corresponding cell contraction. Further details on cardiac contraction and electro-mechanical coupling can be found in [5].

2.1 Nernst Potential

Differences in the ionic concentrations between the interior and the exterior of the cell generates a potential difference across the membrane [2]. We may consider the intracellular space of the cell and the extracellular medium as two reservoirs that separates a certain ion S by a semipermeable membrane, i.e. let us for now consider that the membrane is only permeable to the ion S. The chemical potentials of S inside and outside of the cell are given by:

$$G_{S,i} = RT\ln([S]_i) + zFV_i, \qquad G_{S,e} = RT\ln([S]_e) + zFV_e, \tag{1}$$

where R, T, z and F are the gas constant, temperature, ion charge, and Faraday constant respectively. In a ideal case of equilibrium both chemical potentials are equal giving rise to transmembrane potential difference $(V_i - V_e)$ which depends on the ion concentrations:

$$V_N^S = \frac{RT}{zF}\ln\left(\frac{[S]_e}{[S]_i}\right) \tag{2}$$

which is the definition of the Nernst potential for a given ion S.

For the case of a membrane that is permeable to multiple ion species [2] we have that the equilibrium potential, considering the most important ions inside myocytes, can be approximated by

$$V_r = \frac{g_{Na}V_N^{Na} + g_K V_N^K + g_{Ca}V_N^{Ca} + g_{Cl}V_N^{Cl}}{g_{Na} + g_K + g_{Ca} + g_{Cl}}, \tag{3}$$

where g_S is the permeability of ion S. The equilibrium potential depends on the permeabilities of the ions, which are controlled by the ion channels.

2.2 The Action Potential and Some Basic Properties

From the equilibrium equation presented above we can explain the different phases of the AP in terms of changes of the permeability values of some basic ions, such as K^+ and Na^+. At rest the largest permeability is because of potassium and therefore from Eq. (3): $V_r \sim V_N^K = -96$ mV. It is known that if the cell receives a stimulus above a given threshold the permeability of Na^+ rapidly increases and, again from Eq. (3), if g_{Na} is much larger than the other permeabilities, it results than $V_r \sim V_N^{Na} = +50$ mV and the potential depolarizes to positive values (phase 0). After the

inactivation of sodium channels, dropping the permeability of Na^+, the potassium current produces a deflection of the membrane potential (phase 1) before the Ca^{2+} permeability increases to similar values than K^+ and $V_r \sim (V_N^K + V_N^{Ca})/2$ where $V_N^{Ca} = +134$ mV. The permeability of Ca^{2+} slowly decreases (phase 3) driving the membrane potential back to the $V_r \sim V_N^K$, typical for the rest state (phase 4).

2.3 Membrane Capacitance

Cell membrane separates charges between the interior and the exterior of the cell and therefore it can be interpreted as a capacitor with, $C_m V = q$, where C_m is the membrane capacitance, V is the transmembrane potential and q is the intracellular or extracellular charges. By taking the derivative with respect to time we have that $C_m dV/dt = dq/dt$ is the capacitive current that can be induced by the membrane. In the case a cell is isolated, and assuming a balance of charge, i.e. no charge is being created or destroyed, the sum of the currents from the ion channels, I_{ion} and the capacitive current $C_m dV/dt$ gives rise to a simple electric model presented in Fig. 3. This simple electric models is the basis for the electrophysiological models employed in cardiac modelling:

$$C_m \frac{dV}{dt} = -I_{ion}. \tag{4}$$

However, as we mentioned before, the permeability or conductance of each ion channels varies with time and is known to depend on the transmembrane potential (it may also depend on ion concentrations or other molecules or proteins). In the next section we present models for the so called gating of ion channels, where the

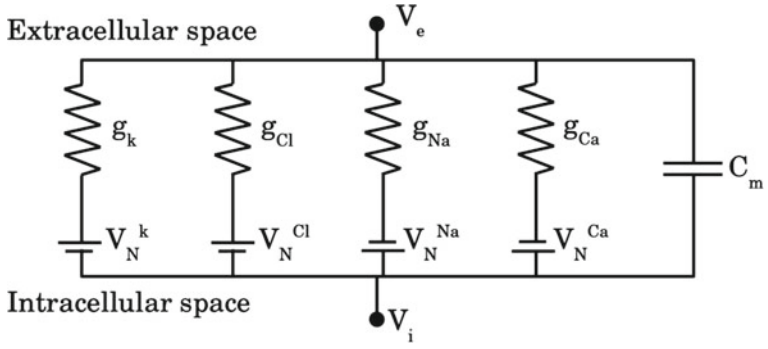

Fig. 3 Equivalent electric circuit model for the cellular membrane. The difference in the transmembrane potential between the extracellular and the intracellular spaces is maintained by the ion current of the different ions through the ion channels, the Nernst potential associated to each ion and the capacitance of the membrane

term gate is commonly used and refers to the fact that ion channels can be opened or closed to the flow of ions.

2.4 Ion Channels

The opening and close of the ion channels are complex processes. Assuming that a particular channel is ohmic the transmembrane potential depends on the Nernst potential of the particular ion V_N^{ion} plus the potential drop due to the current across the ion channel $\rho_{ion} I_{ion}$:

$$V = \rho_{ion} I_{ion} + V_N^{ion}, \tag{5}$$

where ρ_{ion} is the channel resistance, and the transmembrane potential V is the difference between the potentials in the intra- and extracellular media $V = V_i - V_e$. Then, from the previous equation one can obtain the current across the cell membrane for each ion as function of the membrane potential

$$I_{ion} = g_{ion}(V - V_N^{ion}), \tag{6}$$

where $g_{ion} = 1/\rho_{ion}$ is the membrane conductance for that ion, which is in general not constant. In general, the dependence with the potential may be non-linear and a generalization of Eq. (6) is

$$I_{ion} = g_{max} p_O \Phi(V), \tag{7}$$

where $\Phi(V)$ can be a non-linear function of the transmembrane potential, p_O is the proportion of open channels, and g_{max} is the maximum conductance when all the channels are open, i.e. when $p_O = 1$. The most common approach to model p_O is via the use of gating variables, as first proposed by Hodgkin and Huxley, in their pioneering model of AP [6]. For example, consider a K^+ channel that has a time rate $\alpha(V)$ to change from a closed state to an open state; and a time rate $\beta(V)$ to change from an opened state to a closed state. For the case we have many ion channels we can use a deterministic model based on Ordinary Differential Equation (ODE). Since the proportion of closed channels is $1 - p_O$ we have:

$$\frac{dp_O}{dt} = \alpha(V) p_O - \beta(V)(1 - p_O). \tag{8}$$

More complex behaviours, like the one we described for the Sodium channels, which first open and immediately after close (even for the same value of V), can not be described by a single gating variable. Two options are commonly used. The first is to

assume that multiple independent gates have to be opened to let ions flow through the channel. For Sodium channel we could replace Eq. (7) by $I_{Na} = g_{NA}\, p_{Oa}\, p_{Oi} \Phi(V)$, where p_{Oa} is the gating variable associated to activation, p_{Oi} the one associated to inactivation, and both are controlled by equations similar to Eq. (8), but each one with different time rate functions. A more modern approach is to model p_O using a Markov Chain formulation [8].

3 Models of Myocytes

The sinoatrial node (SAN) is the natural pacemaker of the heart and initiates autonomously cardiac electrical activity. APs are produced periodically and propagate along the atria. The wave of AP arrives at the ventricular myocardium through the atrio-ventricular node (AVN) and the Purkinje fibres, depolarizing first the endocardium and proceeding transmurally to the epicardium.

The electrical properties of the heart tissue are very heterogeneous and each type of cells have particular features giving rise to a large diversity on the shape of the action potentials. Next, we present four models for human myocytes: SAN, atria, Purkinje fibres and ventricle. It is worth noting that there are still large differences on the AP shape even in the same region of the heart (e.g. APs are different in the ventricular endocardium and epicardium). In addition, substantial differences can also be found among species. Figure 4 presents a comparison of AP shapes of ventricular myocytes for different species. A small heart, like from a mouse, has higher heart rate and consequently a smaller APD than a human heart [9].

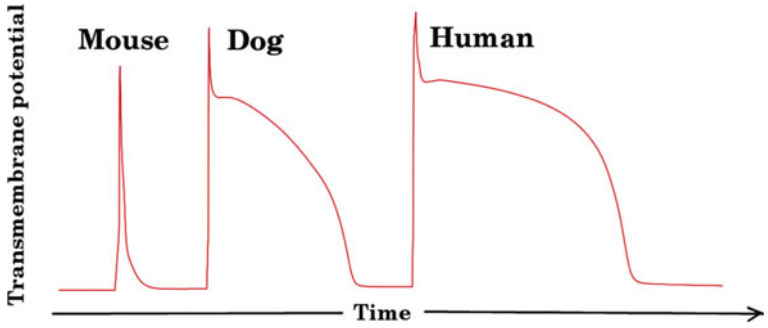

Fig. 4 Comparison of the action potential of a ventricular myocyte of three different animal species. All the action potentials have the same temporal and potential scales. Rest potential is however slightly modified for illustrative reasons. Action potential curves have been generated with program Myokit [7]

3.1 Sinoatrial Node Myocyte

In the right atrium there is a group of cells forming the sinoatrial node which spontaneously depolarize (60–90 min^{-1}). The property of continuous depolarization of such cells (automaticity) triggers repetitive electrical impulses, which defines the periodic contraction of the human heart. Contrary to the majority of the cardiac myocytes, these cells do not experience a rest state or phase 0. A continuous repolarization drives the cell to a hyperpolarization state, see Fig. 5a. At this phase, important ion currents, such as the funny current, I_f, is known to play an important role [10]. The term funny was coined because this current is activated at hyperpolarization and carries mainly Na^+ under physiological conditions. This flux of Na^+ into the pacemaker myocyte will eventually make the transmembrane potential to cross the threshold around -40 mV, where fast depolarization occurs and a new AP is generated.

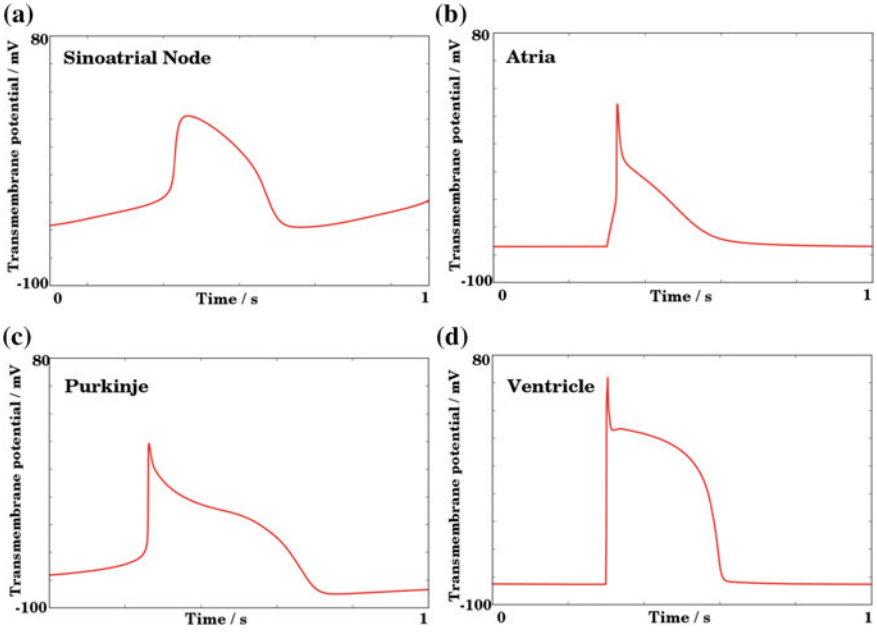

Fig. 5 Transmembrane potential obtained by four models of different cardiac myocytes: Simulated action potentials of a myocyte in the Sinoatrial node (**a**), a myocyte in a human atrium (**b**), a myocyte in human Purkinje fibres (**c**), and a myocyte in a human ventricle (**d**). Action potential curves have been generated with program Myokit [7]

3.2 Atrial Myocyte

Transmembrane potential of a cell in the atrium stays in a resting state of -74 mV when it not being stimulated. When the perturbation of the neighbouring cells and in particular from the sinoatrial node crosses a threshold a fast channel for sodium activates and induces the rapid entrance of sodium into the cell which suddenly depolarizes the cell to values around 20 mV. Phases 2 and 3 of the AP are mixed for atrial cells due to a continuous unbalanced of inward flow of Ca^{2+} and outward flow of K^+. This results in a gradual repolarization to the resting state, see an example in Fig. 5b.

3.3 Purkinje Fiber Myocyte

AP propagation slows down at the AVN node, but speeds up once entering the His bundle followed by the Purkinje fibres. The Purkinje fibres are AP highways that rapidly transport the electric signal to the ventricular myocytes. The myocytes forming the Purkinje fibres are the cells with the longest action potential duration, which arrives to 400 ms, see Fig. 5c to compare it with the other action potentials. In contrast with atrial and ventricular cells the myocytes forming the Purkinje fibres also have a certain automaticity. It means that cells in the Purkinje system are able to sustain low frequency oscillations (15–20 min^{-1}) in case the main pacemaker, the sinoatrial node, fails. Under normal conditions Purkinje fibres do not depolarize spontaneously because they are regularly stimulated at pacing rates higher than their own natural autonomous pacing activity.

3.4 Ventricular Myocyte

Ventricular cells present a stable resting state about -85 mV. Under suprathreshold perturbations the corresponding excitation is due to the opening of the fast Na^+ channels causing a rapid influx of Na^+ ions into the cell. The membrane potential is reversed from negative to positive and arrives to about +60 mV. The posterior deflection of the action potential is due to the movement of K^+ ion together with the inactivation of the fast Na^+ channels. In comparison with a atrial action potential, in ventricle cells the calcium influx is larger and balances the outward flux of K^+. This produces a plateau for about 200 ms, phase 3, which is the main difference between ventricular and atrial action potentials, see Fig. 5d for an example of AP from a model of the human ventricle.

4 Cardiac Tissue

Cardiac cells are electrically connected by special ion channels called gap junctions. These connections permit the propagation of the signal through the tissue and the synchronization of the whole heart. The models of transmembrane potential described in the previous section can be used to implement a model for AP propagation on cardiac tissue. Some particular dynamics observed in tissue models correspond to cardiac arrhythmias observed in the heart.

4.1 Bidomain Modelling

The bidomain model is based on the cable equation. Cardiac tissue is divided in two different regions which are interconnected, the intra- and extracellular regions, see Fig. 6a. The transmembrane potential is considered to vary along the tissue and, due to these variations, intra- and extracellular axial currents per unit length appear [2]:

$$I_i(x) = -g_i[V_i(x+dx) - V_i(x)]/dx, \qquad I_e(x) = -g_e[V_e(x+dx) - V_e(x)]/dx; \quad (9)$$

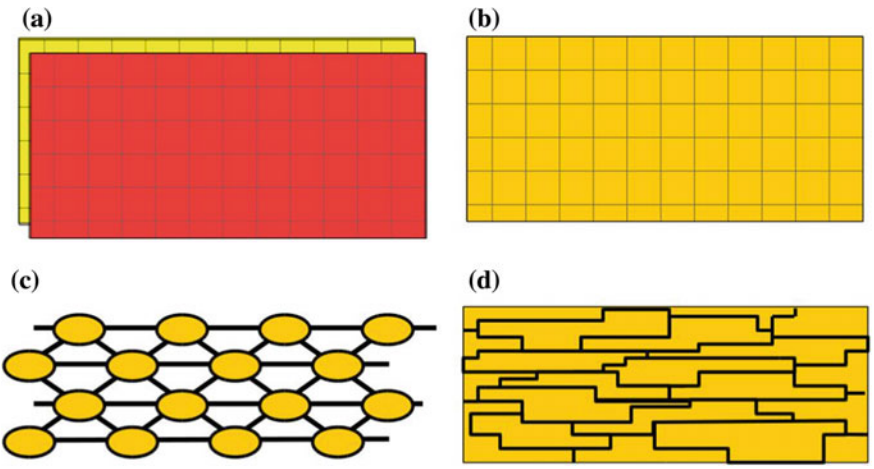

Fig. 6 Different modelling approaches to cardiac tissue: Bidomain model where intracellular (yellow) and extracellular (red) potentials are explicitly considered as two inteconnected continuous models (**a**). Monodomain model where the transmembrane voltage is considered in a continuous model (**b**). Discrete model where the myocyte is approached as an single element and electrically connected to the rest of cells in the tissue (**c**). Heterogeneous approach where single cells are discretized into smaller volume elements and effective and discrete gap junctions take into account cell to cell coupling

where g_i, g_e are the conductances per unit length of the intra- and extracellular media. The sum of the currents entering and leaving a given point of the tissue must be zero, and therefore:

$$I_i(x) - I_i(x + dx) = I_t dx = I_e(x + dx) - I_e(x), \tag{10}$$

where the transmembrane current, I_t is the sum of the ionic and capacitive currents:

$$I_t = p\left(C_m \frac{dV}{dt} + I_{ion}\right), \tag{11}$$

and p is the perimeter of the cell.

In the continuous limit $dx \to 0$, and assuming the 3D case, the previous Eq. (9) become:

$$I_i(x) = -\mathbf{g_i}\nabla V_i, \qquad I_e(x) = -\mathbf{g_e}\nabla V_e, \tag{12}$$

and Eq. (10):

$$I_t = -\nabla \cdot I_i = \nabla \cdot I_e, \tag{13}$$

where $\mathbf{g_i}$ and $\mathbf{g_e}$ are tensors that describe the anisotropy (cardiac fibre direction) of the intra- and extracellular domains, respectively, I_t satisfies:

$$I_t = \chi\left(C_m \frac{dV}{dt} + I_{ion}\right), \tag{14}$$

where χ is the surface to volume ratio of a cell, and I_{ion} is the sum of ion currents, where each one is modelled via equations similar to Eqs. (7–8).

Substituting Eq. (13) in Eq. (14) one obtains the three dimensional bidomain model. Using $V_i = V + V_e$ we have:

$$\chi(C_m \frac{\partial V}{\partial t} + I_{ion}) = \nabla \cdot (\mathbf{g_i}\nabla V) + \nabla \cdot (\mathbf{g_i}\nabla V_e). \tag{15}$$

In addition, from Eq. (13), we have:

$$\nabla \cdot (\mathbf{g_i}\nabla V_i + \mathbf{g_e}\nabla V_e) = \nabla \cdot \left[\mathbf{g_i}\nabla V + (\mathbf{g_i} + \mathbf{g_e})\nabla V_e\right] = 0. \tag{16}$$

Equations (15–16) constitute the bidomain formulation of the cable equation written with the variables V and V_e, which solution depends on the choice of appropriate initial and boundary conditions. The numerical solution of the above system of equations is not a trivial task. In [11] the reader can find a review on sophisticated numerical methods for the solution of the cardiac bidomain equations.

The bidomain model is computationally demanding and it is usually reduced to a more tractable version, the monodomain approach, see next section. However, it is largely assumed that the full bidomain approach is necessary to properly model

defibrillation [12] or to recover patient specific electrocardiogram (ECG) and magnetocardiogram (MCG) signals [13, 14].

4.2 Monodomain Modelling

In one dimension with homogeneous conductances it is always possible to reduce Eqs. (15–16) to a monodomain description. Note that, from Eq. (13), the divergence of the total axial current is zero, from which we obtain the monodomain cable equation.

In three-dimensions, if the anisotropy ratios are equal, i.e. $\mathbf{g_e} = \lambda \mathbf{g_i}$, the bidomain equations can be reduced to a monodomain model, see Fig. 6b. Under such conditions the resulting monodomain equation for the transmembrane potential is:

$$p\left(C_m \frac{\partial V}{\partial t} + I_{ion}\right) = \nabla \cdot (\mathbf{g_o} \nabla V)\,, \tag{17}$$

where we define an effective conductance $\mathbf{g_o} = \lambda/(1+\lambda)\mathbf{g_i}$ [2]. In addition, for the case of plane wave propagation the bidomain equations also simplifies to the modomain equation with an expression for $\mathbf{g_o}$ that depends on the angle between the wave front and the cardiac fibre direction [15, 16].

However, cardiac tissue is known to have tensors with different anisotropy ratio and such equivalence does not hold for the general case. Nevertheless, in most applications of cardiac modelling both models produce similar dynamics [17].

4.3 Discrete Modelling

The previous models of cardiac tissue are based on the continuum and homogenized approach. For the numerical implementation such models are discretized into a grid or a mesh with spatial discretization that can arrive to small values as 100 μm. This is the characteristic size of a single myocyte. Such values may challenge the basis of the continuum and homogenized hypothesis. Therefore, for some applications the discrete nature of the tissue has to be taken into account. The resulting equation is

$$\left(C_m \frac{\partial V_i}{\partial t} + I_{ion}\right) = \sum_j \left(g_{ij}(V_j - V_i)\right), \tag{18}$$

where membrane potential is now a discrete variable V_i, the sum goes for all the neighbours of the cell i and conductivity may depend on the connected cells g_{ij}, see Fig. 6c.

Under slow conduction conditions, velocities are affected by the discreteness [18] and conduction block is observed in the numerical simulations [19]. However, conduction block is not capture by the continuum homogenized models.

Such discrete models have been shown to be convenient for the study of slow propagation, microfibrosis and the complex fractionated electrograms associated to it. A discrete distribution of cells into a square grid and the effects of reduced conductivity has been also analyzed and may induce the formation of ectopic beats [20, 21] or stabilize spiral breakup [22]. More realistic discrete meshes were also used for studies that associated microfibrosis and ectopic beats [23].

Another approach to capture discrete propagation in cardiac tissue is to include a corrector term in the discretization of the continuum homogenized monodomain model [24]. This approach allows the use of the classical continuum homogenized models (with spatial discretization larger than cell size) and yet capture the discrete features of the phenomenon.

4.4 Heterogeneous Modelling

A higher level of detail is obtained with microscopic models of the intracellular space of individual cells. Single cells are discretized at the subcellular level. It permits the description of the actual shape of the myocytes and consider different types of gap junctions depending on the direction of cell [25, 26]. Such models permit the direct simulations of two-dimensional processes at the intra-cellular level and are useful for the study of conduction block [27] and the effects of cardiac fibrosis [23, 28].

There are extensions to three-dimensions [29] and extensions that describe both extracellular and intracellular spaces [30].

5 Action Propagation Dynamics

The contraction of the heart is generated by a single wave of electrical excitation, see Fig. 7b, c for the propagation in a simple model of the ventricles. Tachycardia corresponds to a rotor that accelerates the rate of contraction, and typically is associated to a spiral wave, see Fig. 7d. Fibrillation occurs when the normal electrical activity is masked by higher frequency circulation waves which create small, out-of-phase localized contractions. One or more spiral waves break into multiple waves, see Fig. 7e–h, leading to fibrillation [31].

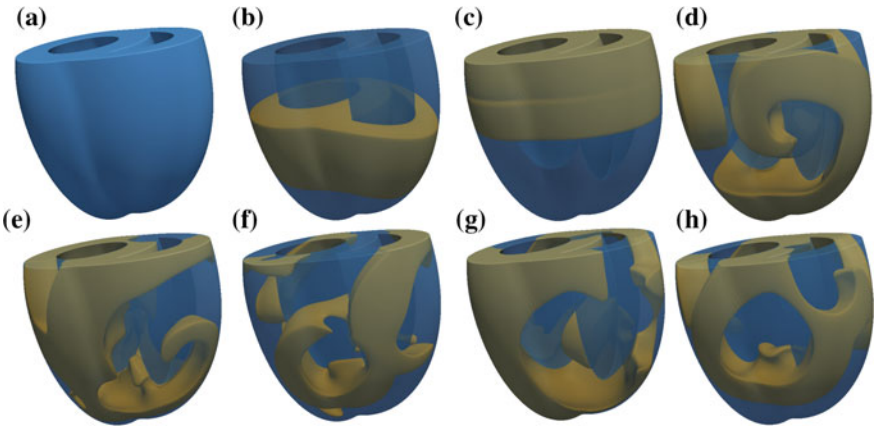

Fig. 7 Numerical simulation of the action potential wave (yellow) with a simple model in a regular domain (blue) with two cavities mimicking the geometrical properties of the ventricles (**a**) A wave is generated in the apex of the ventricles and propagates to the top (**b**, **c**). A secondary stimulus in the ventricles generates a spiral wave (**d**). Spiral wave is unstable (**e**, **f**) and gives rise to multiple spirals which desynchronize the ventricles (**g**, **h**)

5.1 Action Potential Pulse

Myocytes are connected through gap junctions, and action potential propagates along the tissue with roughly constant velocity, see such a wave in a simple model of the two ventricles in Fig. 7b, c.

The collision of two travelling waves in different directions produces their annihilation. However, interactions between consecutive waves travelling in the same direction are common due to the continuous forcing of the whole tissue by the sinoatrial node. The increase of the pacing frequency decreases the diastolic interval (DI) or distance between consecutive pulses. At low pacing frequencies, there is practically no interaction between waves and the wave-train propagates with the single travelling wave velocity, see Fig. 8. On the other hand, at fast pacing, a wave may not be able to propagate because it enters the refractory tail of the preceding wave and propagation is blocked. In between these two situations, waves tune their APD and CV to accommodate the propagation under the influence of the refractory tail of the previous wave, see the decrease of the APD and CV with the DI in Fig. 8, which is inversely proportional to the pacing frequency.

5.2 Tachycardia

Some cardiac arrhythmias appear when the regular synchronous propagation of the action potential along the tissue is disrupted. Tachycardia is a particular case of

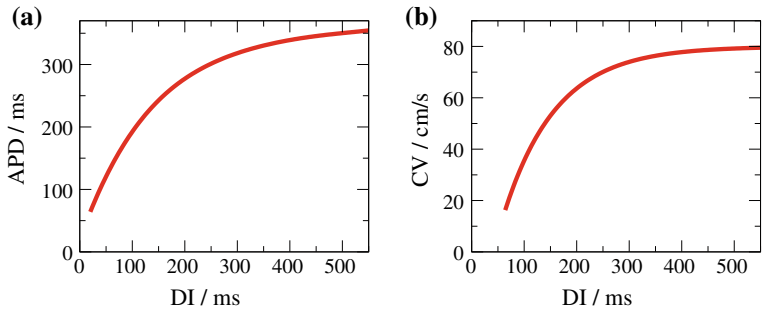

Fig. 8 Restitution curves or dependence of the action potential duration (**a**) and the conductions velocity (**b**) on the diastolic interval, which is related with the pacing frequency in models of the human ventricle

arrhythmia consisting in a fast but regular periodic contraction of the tissue. It has been associated to the appearance of a cardiac reentry around an inhomogeneity in the tissue, for example a vein (anatomical reentry), or it may appear and rotate without the existence of any particular heterogeneity (functional reentry). Reentry in cardiac tissue is often related with the appearance of a rotating spiral wave in the tissue as it has been observed in experiments. The generation of reentry in cardiac tissue is one of the main interests in the modelling of cardiac electrical activity. Next, we highlight two mechanisms of functional reentry observed in experiments and studied in numerical simulations.

The introduction of an extra excitation in the tail of travelling wave is known as ectopic beat. The new excitation cannot propagate in the direction of the refractory tail of the first wave. Hence, it slides along the refractory tail until the tissue becomes again excitable and then rotates giving rise to a spiral. The generation of the spiral wave after the second excitation only occurs during a particular window of time, known as the vulnerability window [32]. If the second perturbation comes too early, a new wave cannot be generated because that part of the tissue is still in the refractory state. If it comes too late, the perturbation generates a circular wave and no reentry is formed.

The alternation of the duration of the action potential at the single cell level results in the interchange of weak and strong contractions of the heart. It only happens when the dependence of the action potential duration on the pacing becomes very strong. An initially periodic wave-train may become unstable and evolve into alternans. In two or three dimensions when one of the pulses is locally too small, it may produce conduction block and initiate the formation of spiral waves due to the displacement of the broken end into the less dramatic region [33]. The probability for the conduction block depends on the pacing frequency of the tissue.

5.3 Fibrillation

One of the most relevant arrhythmias is fibrillation which corresponds to a state where the contraction of many cardiac myocytes are strongly desynchronized in the atria, i.e. atria fibrillation, or, with more dangerous consequences, in the ventricles, i.e. ventricular fibrillation. Electrical defibrillation, the only effective therapy when the ventricles fibrillate, resets the activity of the ventricle by delivering a strong electrical shock. Atrial fibrillation is typically treated by anti-arrhythmic drugs and, for severe cases, with catheter ablation of the most active regions of the atria.

Fibrillation is often attributed to a succession of multiple breakups and pairwise annihilations of spiral waves. Reentry is believed to be a necessary but not a sufficient condition for fibrillation. Computational modelling has shown different mechanisms to explain how the fibrillation can be triggered by a single reentry. For example, alternans can produce localized conduction blocks and break-up waves emitted by a spiral due to the alternation of waves with large and short action potentials. At fast rotation rates, the instability reaches the spiral core and produces a disordered state [34]. On the other hand, high meandering of the spiral waves, typically observed in models of cardiac tissue, may produce the interaction between consecutive waves and produce local conduction block, giving rise to spiral breakup.

Finally, there are other situations which may produce continuous breakup of waves, for example: when the tension of the filament of three-dimensional spirals, i.e. scroll waves, is negative [35]; or when the rotating anisotropy of cardiac fibres induces a scroll wave to breakup [36].

6 Conclusions and Final Remarks

We have described the main features of the computational electrophysiological modelling of the human heart. From the particular shapes of AP of the cardiac cells depending on their location in the heart to the modelling of diverse types of arrhythmias in cardiac tissue. We have also discussed the main methods to couple the electrophysiology of the individual cells to cardiac tissue.

Currently there are complex models of the geometry of the atria and the ventricles taking into account the anisotropy of the cardiac muscle fibres and the heterogeneous properties of the organ. The level of complexity and detail is arriving to permit patient-specific modelling of the electrical activity [37]. Furthermore, models have to couple the electrical part to the deformation of the muscle walls [38].

Therefore, the heart is a multiphysics problem [39] which has to consider the interplay among the electric wave propagation, the mechanics of the muscle contraction and the fluid dynamics inside the cardiac cavities to explain the correct performance of this electromechanical pump. It is also a multiscale problem [40], for example, the wrong operation of a ion channel at small spatial and temporal scales can definitely affect the behaviour on the whole organ. The complete computational modelling may

permit the study of genetic mutations or the effects of drugs, processes, governing small spatial and temporal scales, in the function of the whole macroscopic organ.

Although many improvements on modelling of electrical activity of the heart have been done during the last decades, the complete description of the human heart is still a challenge for cardiac modellers.

Acknowledgements We acknowledge fruitful discussions with professors Blas Echebarria and Markus Bär. This work was partially supported by MINECO of Spain under the Ramon y Cajal program with the grant number RYC-2012-11265, and the Brazilian funding agencies FAPEMIG, CNPq, FINEP and CAPES.

References

1. Zipes D, Jalife J (2013) Cardiac electrophysiology: from cell to bedside. Elsevier, Amsterdam
2. Keener JP, Sneyd J (1998) Mathematical physiology. Springer, New York
3. Malmivuo J, Plonsey R (1995) Bioelectromagnetism: principles and applications of bioelectric and biomagnetic fields. Oxford University Press, Oxford
4. Clayton RH, Bernus O, Cherry EM, Dierckx H, Fenton FH, Mirabella L, Panfilov AV, Sachse FB, Seemann G, Zhang H (2011) Models of cardiac tissue electrophysiology: progress, challenges and open questions. Prog Biophys Mol Biol 104:22–48
5. Pfeiffer ER, Tangney JR, Omens JH, McCulloch AD (2014) Biomechanics of cardiac electromechanical coupling and mechanoelectric feedback. J Biomech Eng 136(2):021007
6. Hodgkin AL, Huxley AF (1952) A quantitative description of membrane current and its application to conduction and excitation in nerve. J Physiol 117(4):500
7. Clerx M, Collins P, de Lange E, Volders PGA (2016) Myokit: a simple interface to cardiac cellular electrophysiology. Prog Biophys Mol Biol 120(1–3):100–114
8. Qu Z, Hu G, Garfinkel A, Weiss JN (2014) Nonlinear and stochastic dynamics in the heart. Phys Rep 543(2):61–162
9. Kaese S, Verheule S (2013) Cardiac electrophysiology in mice: a matter of size. Transgenic models of cardiac arrhythmias and sudden death. 103
10. Campos FO, Davenport MH, dos Santos RW, Nygren A, Giles WR (2013) High heart rate in pregnancy is modulated by augmented expression of an ion channel, HCN-2, in pacemaker tissue. Circulation 20:127
11. Vigmond EJ, dos Santos RW, Prassl AJ, Deo M, Plank G (2008) Solvers for the cardiac bidomain equations. Prog Biophys Mol Biol 1:96
12. Trayanova N, Constantino J, Ashihara T, Plank G (2011) Modeling defibrillation of the heart: approaches and insights. IEEE Rev Biomed Eng 4:89–102
13. dos Santos RW, Kosch O, Steinhoff U, Bauer S, Trahms L, Koch H (2004) MCG to ECG source differences: measurements and a two-dimensional computer model study. J Electrocardiol 1:37
14. Mäntynen V, Konttila T, Stenroos M (2014) Investigations of sensitivity and resolution of ECG and MCG in a realistically shaped thorax model. Phys Med Biol 23:59
15. Roth BJ, Woods MC (1999) The magnetic field associated with a plane wave front propagating through cardiac tissue. IEEE Trans Biomed Eng 11:46
16. dos Santos RW, Koch H (2005) Interpreting biomagnetic fields of planar wave fronts in cardiac muscle. Biophys J 5:88
17. Potse M, Dubé B, Richer J, Vinet A, Gulrajani RM (2006) A comparison of monodomain and bidomain reaction-diffusion models for action potential propagation in the human heart. IEEE Trans Biomed Eng 53(12):2425–2435

18. Rudy Y, Quan W (1987) A model study of the effects of the discrete cellular structure on electrical propagation in cardiac tissue. Circ Res 61(6):815–823
19. Fast VG, Kléber AG (1995) Cardiac tissue geometry as a determinant of unidirectional conduction block: assessment of microscopic excitation spread by optical mapping in patterned cell cultures and in a computer model. Cardiovasc Res 29(5):697–707
20. Cherry EM, Ehrlich JR, Nattel S, Fenton FH (2007) Pulmonary vein reentry—properties and size matter: insights from a computational analysis. Heart Rhythm 4(12):1553–1562
21. Alonso S, Bär M (2013) Reentry near the percolation threshold in a heterogeneous discrete model for cardiac tissue. Phys Rev Lett 110(15):158101
22. Panfilov AV (2002) Spiral breakup in an array of coupled cells: the role of the intercellular conductance. Phys Rev Lett 88(11):118101
23. de Barros Gouvea B, Weber dos Santos R, Lobosco M, Alonso S (2015) Simulation of ectopic pacemakers in the heart: multiple ectopic beats generated by reentry inside fibrotic regions. BioMed Res Int 2015:713058
24. Costa CM, Silva PAA, dos Santos RW (2016) Mind the gap: a semicontinuum model for discrete electrical propagation in cardiac tissue. IEEE Trans Biomed Eng 4:63
25. Spach MS, Heidlage JF (1995) The stochastic nature of cardiac propagation at a microscopic level: electrical description of myocardial architecture and its application to conduction. Circ Res 76(3):366–380
26. de Barros Gouvea B, Sachetto Oliveira R, Meira W, Lobosco M, Weber dos Santos R (2012) Simulations of complex and microscopic models of cardiac electrophysiology powered by multi-GPU platforms. Comput Math Methods Med 2012:824569
27. Prudat Y, Kucera JP (2014) Nonlinear behaviour of conduction and block in cardiac tissue with heterogeneous expression of connexin 43. J Mol Cell Cardiol 76:46–54
28. Hubbard ML, Henriquez CS (2014) A microstructural model of reentry arising from focal breakthrough at sites of source-load mismatch in a central region of slow conduction. Am J Physiol Heart Circ Physiol 306(9):H1341–H1352
29. Spach MS, Barr RC (2000) Effects of cardiac microstructure on propagating electrical waveforms. Circ Res 86(2):e23–e28
30. Roberts SF, Stinstra JG, Henriquez CS (2008) Effect of nonuniform interstitial space properties on impulse propagation: a discrete multidomain model. Biophys J 95:3724–3737
31. Alonso S, Bär M, Echebarria B (2016) Nonlinear physics of electrical wave propagation in the heart: a review. Rep Prog Phys 79(9):096601
32. Qu Z, Garfinkel A, Weiss JN (2006) Vulnerable window for conduction block in a one-dimensional cable of cardiac cells, 1: single extrasystoles. Biophys J 91:793–804
33. Qu Z, Garfinkel A, Chen PS, Weiss JN (2000) Mechanisms of discordant alternans and induction of reentry in simulated cardiac tissue. Circulation 102:1664–1670
34. Karma A (1993) Spiral breakup in model equations of action potential propagation in cardiac tissue. Phys Rev Lett 71:1103
35. Alonso S, Bär M, Panfilov AV (2013) Negative tension of scroll wave filaments and turbulence in three-dimensional excitable media and application in cardiac dynamics. Bull Math Biol 75(8):1351–1376
36. Fenton F, Karma A (1998) Fiber-rotation-induced vortex turbulence in thick myocardium. Phys Rev Lett 81:481
37. Krishnamurthy A, Villongco CT, Chuang J, Frank LR, Nigam V, Belezzuoli E, Stark P, Krummen DE, Narayan S, Omens JH, McCulloch AD (2013) Patient-specific models of cardiac biomechanics. J Comput Phys 244:4–21
38. Oliveira BL, Rocha BM, Barra LPS, Toledo EM, Sundnes J, dos Santos Weber R (2013) Effects of deformation on transmural dispersion of repolarization using in silico models of human left ventricular wedge. Int J Numer Methods Biomed Eng 29:1323–1337

39. Nordsletten DA, Niederer SA, Nash MP, Hunter PJ, Smith NP (2011) Coupling multi-physics models to cardiac mechanics. Prog Biophys Mol Biol 104:77–88
40. Trayanova NA, Rice JJ (2011) Cardiac electromechanical models: from cell to organ. Front Physiol 2:43